NOTICE CONCERNING COPYRIGHT RESTRICTIONS

Effects of Diffusion Potential on Self-Potential Distribution in Geothermal Areas

Tsuneo Ishido[1] and John W. Pritchett[2]

[1]Geological Survey of Japan / AIST
[2]Science Applications International Corporation

Keywords

Self-potential, electrokinetic coupling, diffusion potential, reservoir simulation, natural hydrothermal circulation, production-induced flow

ABSTRACT

Our "EKP Postprocessor" calculates temporal changes in the distribution of electrokinetic self-potential (SP) caused by changes in underground conditions such as pressure, temperature, salinity and liquid-phase saturation as computed by numerical reservoir simulations. Recently, we have extended the EKP Postprocessor to incorporate electrochemical diffusion potential in addition to electrokinetic coupling as SP generation mechanisms. We applied the new postprocessor to computed results from reservoir simulations representing natural hydrothermal circulation and subsequent geothermal fluid production. The present preliminary simulations indicate that diffusion potential effects could account for a substantial part of the natural-state SP anomalies associated with natural hydrothermal circulation systems, especially if a large salinity contrast is present between the hot upflowing thermal fluid and surrounding fresh water. But diffusion potential effects will not play significant roles in production-induced SP changes since production-induced changes in the distributions of fluid chemistry will be minor compared to flow pattern changes, particularly in the early stages of exploitation.

Introduction

In recent years, the SP (self-potential) method has attracted increasing interest in geothermal prospecting and engineering geophysics. Among the various mechanisms which can cause SP, the most important appears to be the electrokinetic (streaming) potential arising from underground fluid flow (e.g., Corwin and Hoover, 1979; Ishido and Mizutani, 1981). Electrokinetic phenomena also receive considerable attention in volcanic studies (e.g., Zablocki, 1976; Ishido, 2004).

The possibility of inducing observable temporal SP changes by geothermal fluid production through electrokinetic coupling was also pointed out by Ishido et al. (1989). This concept suggests that repeat or continuous SP measurements could be a promising technique for geothermal reservoir monitoring. Numerical simulation studies of electrokinetic potentials (Ishido and Pritchett, 1996) also support this possibility.

In addition to the streaming potential, SP anomalies may be generated by subsurface flows of heat or dissolved ions driven by gradients of temperature or chemical concentration respectively. The voltages generated by such flows are called thermoelectric and electrochemical diffusion potentials (e.g., Corwin and Hoover, 1979). Modeling studies concerning SP anomalies caused by these effects have not been carried out for many geothermal systems, but Darnet et al. (2004) analyzed the relative contribution of these effects to the SP anomalies observed at the Soultz EGS site. In this paper, we focus on the diffusion potential and present the results of numerical simulations of SP generation through electokinetic and diffusion potential mechanisms using the extended EKP postprocessor.

EKP-Postprocessor Extension to Treat Diffusion Potential

The original "EKP (*Electro-Kinetic Potential*) Postprocessor" (Ishido and Pritchett, 1999) calculates space/time distributions of electrokinetic potentials resulting from histories of underground conditions (pressure, temperature, salt concentration, liquid-phase saturation, etc.) computed by multi-phase multi-component unsteady geothermal reservoir simulations. The basic equation solved by the postprocessor is:

$$-\nabla\cdot \mathbf{I}_{cond} = \nabla\cdot \mathbf{I}_{drag} \quad (1)$$

where $\mathbf{I}_{cond}$ ($= -L_{ee}\nabla\phi$) is a conduction current density caused by the electric potential gradient ($\nabla\phi$), and $\mathbf{I}_{drag}$ ($= -L_{ev}\nabla\xi$) is a drag current density caused by charges moved by fluid flow (due to the driving force $\nabla\xi$) through electrokinetic coupling (here, L_{ee}: electrical conductivity of fluid/rock composite, and L_{ev}: cross-coupling coefficient).

In the extended postprocessor, a new source term due to the diffusion potential (e.g., Bockris and Reddy, 1998) is added to the right hand side of equation (1):

$$-\nabla\cdot\mathbf{I}_{\rm cond} = \nabla\cdot\mathbf{I}_{\rm drag} + \nabla\cdot\mathbf{I}_{\rm diff} \tag{2}$$

Here,

$$\mathbf{I}_{\rm diff} = -F_m^{-1}S_L^n\sum_i(\nu_{i+}z_{i+}D_{i+} - \nu_{i-}z_{i-}D_{i-})F\nabla c_i \tag{3}$$

where F_m is the electrical formation factor, S_L is the liquid-phase saturation and n is assumed to be 1 in the present study; $\nu_{i\pm}$, $z_{i\pm}$, and $D_{i\pm}$ are the stoichiometric number, valence and diffusion coefficient of the positive/negative ion of ionic species i; F is Faraday's constant; and c_i is the concentration of species i. In the present postprocessor the temperature dependency of the diffusion coefficient is given on the basis of the Stokes-Einstein relation:

$$D_\pm\text{: diffusivity } [\mathrm{m^2s^{-1}}] \;=\; D_\pm(298)\frac{T}{298}\frac{\mu(298)}{\mu(T)} \tag{4}$$

where $D_\pm(298)$ is the diffusion coefficient of the positive or negative ion for a dilute solution at 298 K, for which values are available in chemical handbooks, and μ is the liquid viscosity.

If the contribution of the surface conductivity is negligible, the electrical conductivity of a porous medium for a z:z valent electrolyte is given using the ionic mobility, $u_\pm=(zF/RT)D_\pm$:

$$\mathrm{L_{ee}} = F_m^{-1}S_L^n(u_+ + u_-)zF\ c \tag{5}$$

Using (3) and (5) together with the conservation of electric charge: $\mathbf{I}_{\rm cond}+\mathbf{I}_{\rm diff}=0$, the so-called Plank-Henderson equation for diffusion potentials is obtained for porous media under several simplified conditions:

$$\varphi_2-\varphi_1 = -\frac{RT}{zF}(t_+ - t_-)\ln\left(\frac{c_2}{c_1}\right) \tag{6}$$

where $t_\pm$ is the transport number given by:

$$t_\pm = \frac{u_\pm}{u_+ + u_-} = \frac{D_\pm}{D_+ + D_-} \tag{7}$$

Equation (6) gives the following diffusion potential for NaCl solution at 25 °C:

$$\varphi_2-\varphi_1 \approx 12.3\ \times\ \log(\mathrm{c_2}/c_1)\ \mathrm{mV}$$

Although the above formulation (3) for the diffusion potential is only approximate, we used it in the present preliminary studies. In cases where the surface conductivity through the electrical double layer is dominant, the effective transport number will be quite different from that given by (7) (Revil, 1999). Such effects need to be considered in the future studies.

The extended EKP postprocessor simulates electric potentials caused by subsurface fluid flow and salt concentration gradient using a two-step process. First, it calculates the distributions of pertinent parameters such as $\mathrm{L_{ee}}$, $\mathrm{L_{ev}}$, $D_\pm$, $\mathbf{I}_{\rm drag}$ and $\mathbf{I}_{\rm diff}$ from the reservoir-simulation results using the same spatial grid used for the reservoir simulation calculation (called the RSV-grid hereafter). Second, the postprocessor calculates the electrical potential (ϕ) distribution by solving Poisson's equation (2) numerically, using a finite-difference grid (hereafter called the SP-grid) which is usually much greater in spatial extent than the RSV-grid, and within which the RSV-grid is embedded.

Within the portion of the SP-grid overlapped by the RSV-grid, the distribution of electrical conductivity is obtained directly from RSV-grid values. Elsewhere within the SP-grid, the electrical conductivity distribution is user-specified and time-invariant. Ordinarily, zero normal potential gradient ("Neumann" condition) on the ground surface (upper surface) and zero potential ("Dirichlet" condition) along the bottom and vertical sides of the SP-grid are imposed. Equation (2) is solved numerically for the electrical potential distribution using a Gauss-Seidel iteration procedure which involves intermittent automatic optimization of the overrelaxation factor.

Illustrative Case

We will describe illustrative computations which have been carried out using the extended EKP postprocessor. The mathematical reservoir model simulates both natural hydrothermal convection and production effects.

A two-dimensional computational grid was used; it extends from x = -5 km to +5 km and y = 3 km depth to 0 km depth in the horizontal and vertical directions, respectively. Horizontal block size is 100 m in the central region between x = ± 2 km and 250 m elsewhere. In the vertical direction, the topmost layer adjacent to the earth surface is 10 m thick. The next layer down is 90 m thick. Nineteen additional 100 m layers span the depth to 2 km, and then four additional 250 m layers are added to reach the lower grid boundary at 3 km depth. The entire volume is subdivided into two sub-regions: a "central" region (extending from x = -3 km to +3 km in the horizontal direction and shallower than 2.5 km depth except for the central 200 m horizontal interval, where it extends downward to the lower grid boundary) and the remaining "peripheral" regions. The permeability is 10^{-14} and 10^{-15} $\mathrm{m^2}$ for the "central" and "peripheral" regions, respectively, and the porosity is 0.1 for both regions. All exterior boundaries except the top surface are closed; pressure and temperature are maintained at 1 bar and 20 °C respectively along the top boundary. Any "fresh water" which flows downward into the grid through the top surface is treated as a dilute NaCl solution (0.00032 mass fraction).

A source of high-temperature (280 ºC) "magmatic water" (containing 0.032 and 0.0032 dissolved NaCl mass fraction in cases 1 and 2, respectively) was imposed at the center of the lower grid boundary (x = 0 and y = 3 km depth); the temporal evolution of the hydrothermal convection system was simulated for constant source flow-rate using the STAR simulator (Pritchett, 1995). Initial conditions were all-liquid, isothermal (20 ºC), isohaline (0.00032 mass fraction NaCl), and hydrostatic. After several thousand years the system reached a steady state in which freshwater downflow in the peripheral region and hot saline water upflow in the central region take place. Figure 1 (a) shows the distributions of temperature, pressure, NaCl mass fraction, and the two-phase steam/water zone after 10^4 years of stabilization.

The STAR simulator was next used to perform a several-hundred-day forecast of the consequences of production for both cases 1 and 2, starting from the natural-states. All boundary conditions and rock properties are the same as those used to calculate the

natural-states. Fluid is withdrawn from two central blocks at 1 km depth at a fixed total flow rate of 720 tons/hour-km. No re-injection of waste fluid takes place in these calculations. Temperature, pressure, NaCl mass fraction and the two-phase zone after 100 days of field operation are shown for Case 1 in Figure 1 (b).

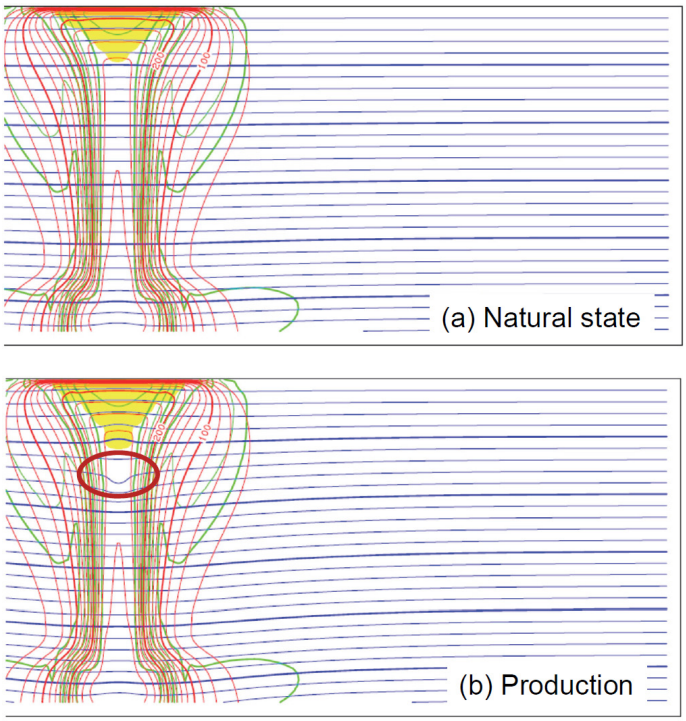

Figure 1. Distributions of temperature (red contours with 20 °C interval), pressure (blue contours with 10 bar interval), NaCl mass fraction (green contours with 0.005 interval) and two-phase region (yellow color) under natural (a) and exploited (b) conditions for case 1. The cross sectional area shown is x = -1 km to 5 km and y = 3 km depth to zero depth in the horizontal and vertical directions, respectively. Region of fluid production near 1 km depth is indicated by heavy red outline in (b).

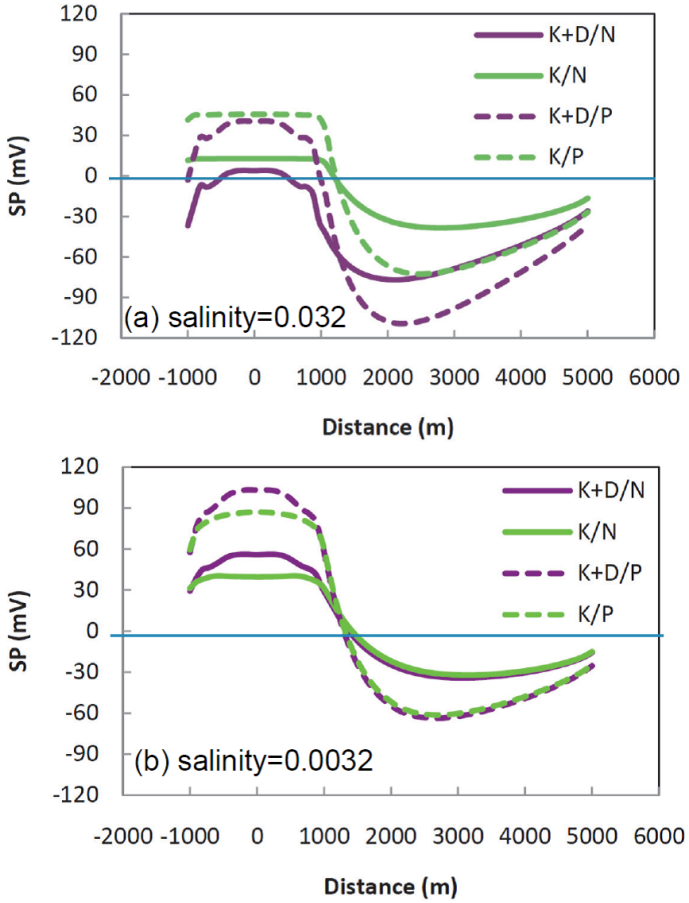

Figure 2. Calculated ground-surface SP distribution for (a) case 1 and (b) case 2. Curves denoted by "K/N" and "K/P" are the results taking only electrokinetic coupling into account for the natural and production states, respectively. Curves denoted by "K+D/N" and "K+D/P" are the results taking into account both electrokinetic coupling and diffusion potential for the natural and production states, respectively.

The results of the extended EKP postprocessor calculations are shown in Figure 2. Electrokinetic (EK) coupling alone causes SP anomalies of positive and negative polarity in the central and peripheral regions, respectively for the natural state in both cases 1 and 2. Although the magnitude of the peripheral negative anomaly is the same for the two cases, that of the central positive anomaly is smaller for Case 1 owing to the relatively high electrical conductivity of the more saline hot water in that case.

If we take into account the diffusion potential mechanism in addition to the EK coupling, the difference in SP between the central and peripheral regions increases by about 30 and 16 mV for cases 1 and 2 respectively. This additional potential difference is consistent with the above theoretical value for the diffusion potential due to salinity gradient (equation [6]). As a result, the SP distribution over the entire region becomes quite similar for the two cases when diffusion potential effects are taken into consideration.

Calculated SP changes associated with fluid production for 100 days are also shown in Figure 2. In both cases, the difference in SP between the central and peripheral regions is substantially increased (by about 60 and 80 mV for cases 1 and 2 respectively for the parameter values chosen). This change, which increases gradually with further production for several hundred days, is mainly caused by EK coupling, since the magnitude of the change is the same for the cases with and without the diffusion potential effects as seen in Figure 2. The appearance of this production-induced SP change at the earth surface is explained by dipole current sources of the total potential for EK coupling (e.g., Fitterman, 1978) induced along the interface between the central saline region of lower streaming potential coefficient magnitude and the peripheral region of higher streaming potential coefficient magnitude (Figure 3). The contribution of the diffusion potential to the temporal change in potential is very minor since the salinity distribution does not change very much from the natural state during production.

In the above cases, the effect of the diffusion potential depends substantially on the pore fluid salinity at the earth surface, where the measuring (non-polarizing) electrode makes contact. For example, if a local shallow freshwater region is present in the middle of the upflow region, the diffusion potential mechanism does not contribute to the potential difference between the local region and the peripheral freshwater region as shown in Figure 4.

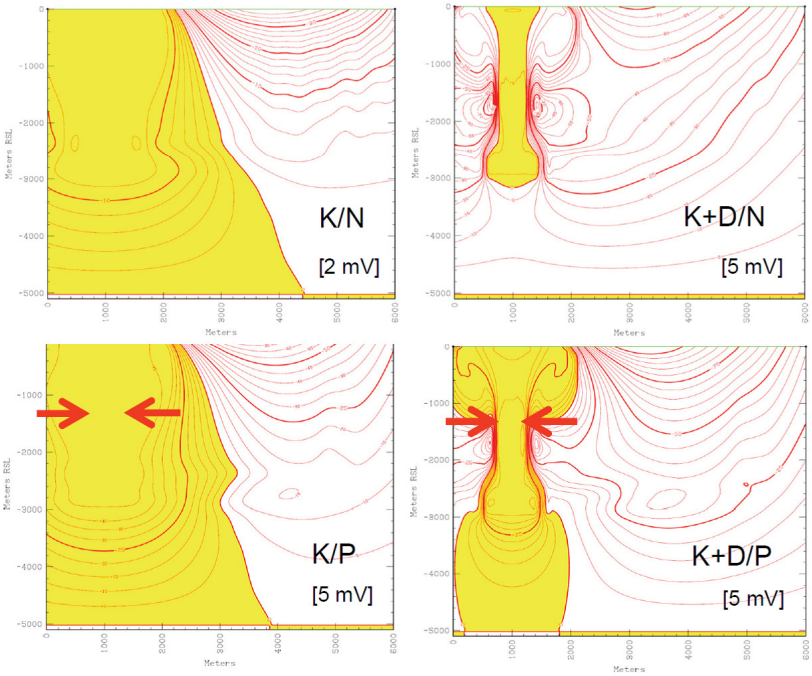

Figure 3. Vertical cross-sectional contour plots of electric potential distribution for case 1. Yellow indicates the region of positive potential. Red arrows schematically show the total potential source induced by fluid production along the interface between regions of central lower and peripheral higher magnitude of the streaming potential coefficient. Contour interval is shown in brackets for each panel.

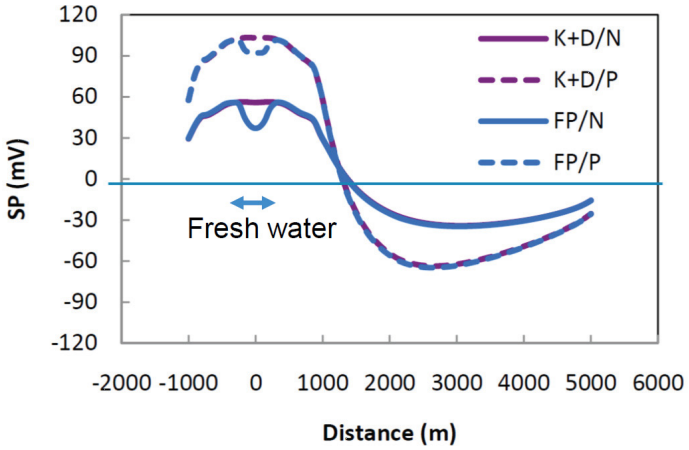

Figure 4. Calculated ground-surface SP distribution for case 2. Curves denoted by "K+D/N" and "K+D/P" are the same results shown in Figure 2(b). Curves denoted by "FP/N" and "FP/P" are the results for a case with the presence of a shallow local freshwater zone in the middle of the upflow region.

Field Observation

The Nigorikawa caldera is located in the southern part of Hokkaido Island, Japan. The diameter of the caldera is about 3 km and various fumaroles and hot springs are located within the northern half of the caldera floor. The thermal waters are neutral and contain substantial HCO^{3-}. The NaCl mass fraction ranges from 0.0001 to 0.01. Figure 5 shows the measured SP profile across the caldera (Ishido, 1981). SP is high inside the caldera where the upflows take place, but the surrounding area is characterized by negative SP anomalies. These features are well reproduced by the present simple two-dimensional model either with EK coupling alone or with a combination of EK and diffusion potential effects (Figure 2). However, the observed local SP highs within the caldera near the fumaroles are better explained by the model incorporating both effects and assuming the presence of local freshwater areas (Figure 4).

The Mori geothermal power plant was built in the Nigorikawa caldera in 1982 and has been in continuous operation since. Comparing the results of SP surveys in 1978, 1981 and 1984, Ishido et al. (1989) found a production-induced SP change. The most obvious change between 1981 and 1984 took place in peripheral areas of the caldera floor; a decrease in SP of about 40 mV was observed along the northern and eastern caldera rim. In contrast to this, a slight increase in SP was observed in the central caldera floor. These features are consistent with the case 1 results shown in Figure 2(a). Subsequently, Yasukawa et al. (2005) observed SP changes associated with a one-month field-wide shut-in of the Mori production and re-injection wells in 2000. The 2000 SP changes are consistent with the changes observed between 1981 and 1984. Yasukawa et al. also interpreted these changes by numerical simulation of EK effects.

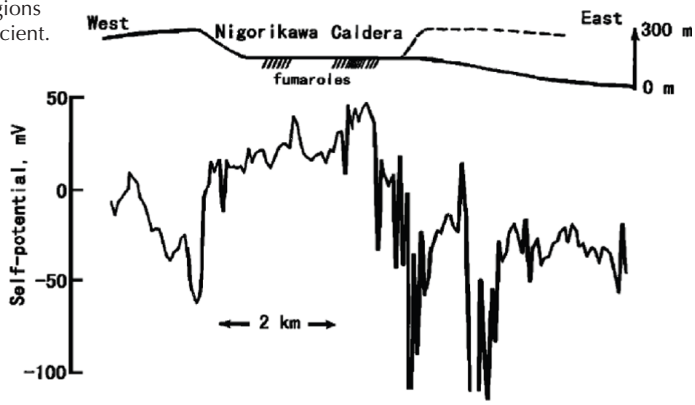

Figure 5. Topographic section and SP profile across the Nigorikawa caldera in 1978 (after Ishido, 1981).

Concluding Remarks

In addition to electrokinetic (EK) coupling, several other effects such as thermoelectric coupling and chemical diffusion potential cannot be ruled out as possible causes of self-potential anomalies in geothermal fields. In the present preliminary study relative contributions of the diffusion potential to the EK effects were examined. The present simulations indicate that the diffusion potential effects could account for a substantial part of the natural-state SP anomalies associated with hydrothermal circulation, particularly if a large salinity contrast is present between the hot upflowing geothermal fluid and surrounding cool groundwater. However, EK phenomena are almost certainly responsible for the production-induced changes in SP which take place after a field is developed. No other effects will play significant roles, since production-induced changes in the distributions of fluid chemistry and temperature will be minor compared to flow pattern changes, especially in the early stages of exploitation.

References

Bockris, J.O'M. and A.K.N. Reddy, 1998. "Modern Electrochemistry: Ionics." 2nd ed., pp.767, Plenum Press.

Corwin, R.F., and D.B. Hoover, 1979. "The Self-Potential Method in Geothermal Exploration." Geophysics, 44, pp.226-245.

Darnet, M., A. Maineult and M. Guy, 2004. "On the Origins of Self-Potential (SP) Anomalies Induced by Water Injections into Geothermal Reservoirs." Geophys. Res. Lett., 31, L19609, doi:10.1029/2004GL020922.

Fitterman, D.V., 1978. "Electrokinetic and Magnetic Anomalies Associated with Dilatant Regions in a Layered Earth." J. Geophys. Res., 83, pp.5923-5928.

Ishido, T., 1981. "Streaming Potential Associated with Hydrothermal Convection in the Crust: a Possible Mechanism of Self-Potential Anomalies in Geothermal Areas." J. Geotherm. Res. Soc. Jpn, 3, pp.87-100 (in Japanese with English abstr.).

Ishido, T., 2004. "Electrokinetic Mechanism for the "W"-Shaped Self-Potential on Volcanoes." Geophys. Res. Lett., 31, L15616, doi:10.1029/2004GL020409.

Ishido, T. and H. Mizutani, 1981. "Experimental and Theoretical Basis of Electrokinetic Phenomena in Rock Water Systems and its Applications to Geophysics." J. Geophys. Res., 86, pp.1763-1775.

Ishido, T. and J.W. Pritchett, 1996. "Numerical Simulation of Electrokinetic Potentials Associated with Natural and Production-Induced Hydrothermal Fluid Flows." GRC Transactions, 20, pp.323-329.

Ishido, T. and J.W. Pritchett, 1999. "Numerical Simulation of Electrokinetic Potentials Associated with Subsurface Fluid Flow." J. Geophys. Res., 104, pp.15247-15259.

Ishido, T., T. Kikuchi and M. Sugihara, 1989. "Mapping Thermally Driven Upflows by the Self-Potential Method." in Hydrogeological Regimes and Their Subsurface Thermal Effects, Geophys. Monogr., 47, IUGG Vol. 2, edited by A.E. Beck, G. Garven, and L. Stegena, pp.151-158, AGU.

Pritchett, J.W., 1995. "STAR: a Geothermal Reservoir Simulation System." in Proc. World Geothermal Congress '95, Florence, pp.2959-2963.

Revil, A., 1999. "Ionic Diffusivity, Electrical Conductivity, Membrane and Thermoelectric Potentials in Colloids and Granular Porous Media: a Unified Model." J. Colloid Interface Sci., 212, pp.503-522.

Yasukawa, K., T. Ishido and I. Suzuki, 2005. "Geothermal Reservoir Monitoring by Continuous Self-Potential Measurements, Mori Geothermal Field, Japan." Geothermics, 34(5), pp.551-567.

Zablocki, C.J., 1976. "Mapping Thermal Anomalies on an Active Volcano by the Self Potential Method, Kilauea, Hawaii." in Proc. 2nd U.N. Symposium on the Development and Use of Geothermal Resources, 2, pp.1299-1309, San Francisco.